Digital decoding of in-line holograms

Levent Onural
Bilkent University
Electrical and Electronics Engineering Department
P.K. 8, 06572 Maltepe
Ankara, Turkey

Peter D. Scott
State University of New York at Buffalo
Electrical and Computer Engineering Department
Laboratory for Power and Environmental Studies
Amherst, New York 14260

Abstract. Digitally sampled in-line holograms may be linearly filtered to reconstruct a representation of the original object distribution, thereby decoding the information contained in the hologram. The decoding process is performed by digital computation rather than optically. Substitution of digital for optical decoding has several advantages, including selective suppression of the twin-image artifact, elimination of the far-field requirement, and automation of the data reduction and analysis process. The proposed filter is a truncated series expansion of the inverse of that operator that maps object opacity function to hologram intensity. The first term of the expansion is shown to be equivalent to conventional (optical) reconstruction, with successive terms increasingly suppressing the twin image. The algorithm is computationally efficient, requiring only a single fast Fourier transform pair.

Subject terms: in-line holography; digital holography; image processing; inverse filtering.

Optical Engineering 26(11), 1124-1132 (November 1987).

CONTENTS

1. INTRODUCTION

An in-line hologram (see Fig. 1) captures, with high resolution, the three-dimensional location and cross-sectional morphology of every object within a thick volume (corresponding to several thousand depths of field of conventional photography[1]). Since object and reference waves are the diffracted and undiffracted components of a single beam, with no additional optics required, the recording system is remarkably simple and well suited for adverse industrial and field environments.

In spite of these attractive features, in-line holography found few practical applications from its discovery until the mid-1960s, when Thompson demonstrated the effectiveness of the technique in visualizing particle fields and aerosols.[2-4] The principal drawback that limited application of in-line holography is an undesirable defocused twin image overlaid on the desired focused image in the standard reconstruction. Especially in holograms recorded in the Fresnel zone, image and twin image intermingle in complex patterns, causing difficulty in defining the correct object boundaries. Thompson pointed out that in reconstructions from holograms recorded in the Fraunhofer zone, however, these two image components are quite distinguishable and thus easily discerned. Restricting attention to ensembles of small compact objects such as particles and droplets, it is possible to locate the holographic medium in both the Fraunhofer zone of the individual objects and the Fresnel zone of the ensemble. This alleviates the twin-image problem, yet the cross-section planar locations of the particles can be easily detected directly from the hologram. Although the twin image is present with undiminished amplitude, its relative lack of interference with object boundary visualization has permitted particle field and aerosol analysis to develop as the most prominent application of in-line holography. Useful reviews of progress in particle field holography include Refs. 1, 5, and 6.

Efforts to alleviate the twin-image problem in a more general setting, while dating nearly from the inception of holography itself, have met with limited success. Early optical methods are reviewed by Collier et al.[7] Here we present an alternative remedy to the twin-image problem, one that does not require that in-line holograms be recorded in the Fraunhofer zone of individual particles. The overall reconstruction process is treated as a signal processing problem, and the solution is implemented digitally. Rather than enforce restrictions that make the twin image look different from the desired

Paper 2321 received Aug. 4, 1986; revised manuscript received June 10, 1987; accepted for publication June 15, 1987; received by Managing Editor June 17, 1987.

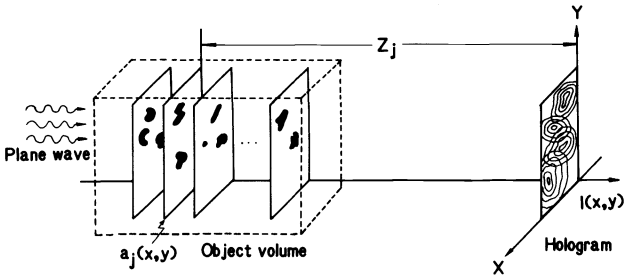

Fig. 1. In-line hologram recording: multiplanar model.

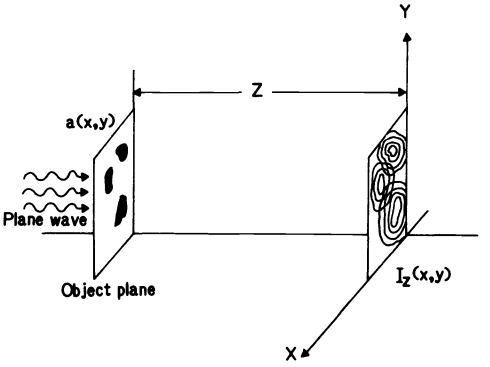

Fig. 2. In-line hologram recording: single object plane.

focused image component, we digitally filter the sampled hologram to selectively suppress the undesired component of the resulting reconstruction while preserving the desired component. This eliminates confusion between object and twin image even in circumstances that challenge the far-field distinguishability assumption, such as dense ensembles of irregular particles where random phase relations between adjacent twin images create patterns difficult to distinguish from actual particles. Removal of the Fraunhofer (far-field) requirement further permits broad dispersions of particle sizes within a single hologram, thus extending the range of application of the in-line technique to scenes in which it is not possible to record in the far field of the larger particles while adequately resolving each smaller one. In addition, the digital decoding process presented in this paper represents progress toward automation of the data reduction and analysis process. Particle field and aerosol holograms tend to be data-intensive, and the need for objective, automated data reduction has often been cited (see, for example, Refs. 8 and 9).

Decoding of in-line holograms by digital signal processing technique is a new and promising direction. An early approach used direct clipping for artifact suppression.[10] A more recent study employs a phase retrieval algorithm to iteratively reconstruct the phase component, which is lost during the optical recording of the hologram.[11] Once the phase is obtained with the help of constraints, the reconstruction is free of the undesired twin image. However, a drawback of such iterative algorithms, including the phase retrieval, is the considerable number of iterations and computation time required.

The technique presented in this paper uses a truncated inverse filtering approach that is computationally efficient and is effective in suppressing the twin image in the reconstructions. Once the desired image has been reconstructed, further image processing may be done for finding the peripheral contours of the objects captured in the hologram.

2. PROBLEM FORMULATION FOR 2-D SYSTEM REPRESENTATION

The signals and transforms of in-line holography may be derived and expressed from a variety of perspectives emphasizing, variously, physical optics,[12-14] system theoretic,[13] or particle field application[15] aspects. Here we adopt a notational scheme based on the observation that planar holograms and their planar reconstructions are ensembles of two-dimensional signals and thus are amenable to sampling, filtering, and other standard two-dimensional signal processing operations.

An in-line hologram is captured as in Fig. 1. A plane wave of coherent radiation (wavelength λ) propagating in the z-direction illuminates a sample volume containing multiple small objects that diffract this incident field. Without loss of generality, we assume the phase of the plane wave at the hologram plane to be zero. Each object is taken to be vanishingly thin in the z-direction, i.e., a pure cross-sectional object, so that the ensemble of these objects may be described by a set of two-dimensional opacity functions $a_j(x,y)$, $j = 1, 2, \ldots, N$. Here, $a_j(x,y) = 1$ if an opaque particle in the plane at a distance z_j from the hologram plane covers the point (x,y); $a_j(x,y) = 0$ if the z_j plane is transparent at (x,y); for general objects $a_j(x,y)$ is a complex function. However, to guarantee convergence of the algorithm to be introduced in the next section, we restrict the object distribution to be strictly real (for instance, opaque particles). Uncertain convergence for objects of variable phase is a significant limitation to the algorithm in its present form.

If all objects occupied the single plane at a distance z from the hologram plane (see Fig. 2) with opacity function $a(x,y)$, then the scalar field produced at the hologram plane could be expressed as the Fresnel-Kirchhoff integral,

$$\psi_z(x,y) = B\exp(-jkz)\int_{-\infty}^{\infty}\int_{-\infty}^{\infty}[1 - a(\xi,\eta)] \times \left(\frac{\exp(jkz)}{j\lambda z}\exp\left\{j\frac{\pi}{\lambda z}[(x-\xi)^2 + (y-\eta)^2]\right\}\right)d\xi d\eta, \quad (1)$$

where $k = 2\pi/\lambda$, B is the amplitude of the incident plane wave (hereafer taken as unity), and $-kz$ is the phase of the illuminating wave at the object plane. Denoting the convolution kernel of this integral as

$$\bar{h}_z(x,y) \triangleq \frac{\exp(jkz)}{j\lambda z}\exp\left[j\frac{\pi}{\lambda z}(x^2 + y^2)\right], \quad (2)$$

we can express the field Eq. (1) more compactly as the 2-D convolution

$$\psi_z(x,y) = \exp(-jkz)\,[1 - a(x,y)] ** \bar{h}_z(x,y) \quad (3)$$

of the inpulse response $\bar{h}_z(x,y)$ with the 2-D input signal $\exp(-jkz)[1 - a(x,y)]$. It is convenient to define another impulse response $h_z(x,y)$, related to $\bar{h}_z(x,y)$ by a phase shift:

$$h_z(x,y) \triangleq \exp(-jkz)\bar{h}_z(x,y) = \frac{1}{j\lambda z}\exp\left[j\frac{\pi}{\lambda z}(x^2+y^2)\right] . \quad (4)$$

With this definition, Eq. (3) becomes

$$\psi_z(x,y) = [1 - a(x,y)] ** h_z(x,y) . \quad (5)$$

Denoting the modulus squared (intensity) of the resultant field as $I_z(x,y)$ and using the identity $1 ** h_z(x,y) = 1$ (see the appendix),

$$I_z(x,y) = \psi_z(x,y)\psi_z^*(x,y) \quad (6)$$

becomes

$$I_z(x,y) = |1 - a(x,y) ** h_z(x,y)|^2 . \quad (7)$$

Since the film used to record the hologram is sensitive to the intensity of the field on the hologram plane, $I_z(x,y)$ will also be referred to as the hologram of $a(x,y)$ taken at a distance z. The system model corresponding to Fig. 2 is shown in Fig. 3. Expanding Eq. (7), we obtain

$$I_z(x,y) = 1 - a^*(x,y) ** h_z^*(x,y) - a(x,y) ** h_z(x,y) + |a(x,y) ** h_z(x,y)|^2 . \quad (8)$$

When the hologram is reilluminated, the first term will lead to a uniform component, the second and third terms to the real and virtual images of the object distribution, respectively, and the final term to a nonlinear component. For high quality optical reconstructions, this final term must be dominated by the other image components. This is conventionally guaranteed by requiring that the rms power in the undiffracted (directly transmitted) reference wave over the hologram be much greater than that of the diffracted object wave; i.e., $0 < \|a(x,y)\|_{rms} \ll 1$. Under this assumption, the final term in Eq. (8) is dominated in the rms sense over the hologram by each of the other terms and may be neglected.

To guarantee convergence of the result of the twin-image elimination algorithm to the desired object distribution, we hereafter assume each $a_j(x,y)$ to be a real-valued function. As a consequence of this assumption, the algorithm of Sec. 3 cannot be used for general objects with complex-valued transmittance functions.

Dropping the dominated last term of Eq. (8) and merging the preceding pair of terms with $a(x,y)$ (assumed real valued), we obtain

$$I_z(x,y) = 1 - a(x,y) ** 2\mathrm{Re}\{h_z(x,y)\} . \quad (9)$$

Under these assumptions, the in-line hologram $I_z(x,y)$ is seen to be the shifted output of a two-dimensional linear filter with input $-a(x,y)$ and impulse response $g(x,y) \triangleq 2\mathrm{Re}\{h_z(x,y)\}$, as shown in Fig. 4.

If the object distribution occupies several planes instead of a single plane, multiple diffraction effects must be considered. For instance, the radiation incident on the second object plane is the superposition of the propagated plane wave originally incident on the first object plane and the object wave diffracted by the first plane. However, under the assumption that the diffracted wave has much less energy than the transmitted plane wave, the field incident on the second object plane is

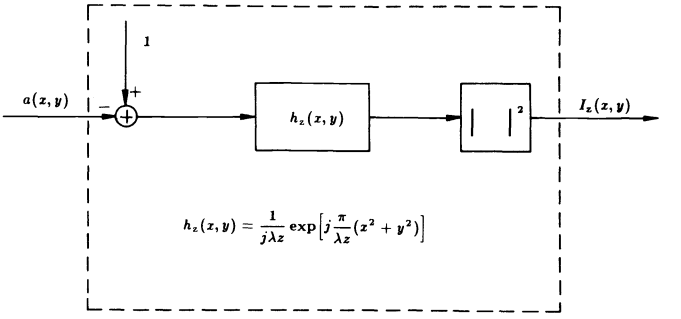

Fig. 3. 2-D system model corresponding to Fig. 2.

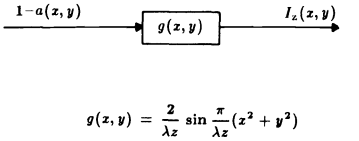

Fig. 4. Linear system approximation to the system of Fig. 3; a(x, y) is real valued.

dominated by its plane wave component and may be computed as above. The field on the hologram plane is then

$$\psi(x,y) = 1 - \sum_j a_j(x,y) ** h_{z_j}(x,y) , \quad (10)$$

where the sum is taken over all object planes, and taking the modulus squared (with dominated nonlinear components dropped), the resulting hologram is

$$I(x,y) = 1 - \sum_j a_j(x,y) ** 2\mathrm{Re}\{h_{z_j}(x,y)\} . \quad (11)$$

Comparing Eqs. (11) and (9), the hologram in the general multiplanar case is just a shifted superposition of holograms of planar object distributions.

For simplicity, we will derive the reconstruction and twin-image suppression formulas for the single plane case. It is straightforward to expand these formulas for multiplanar object distributions.

Conventionally, reconstruction is performed by reilluminating the developed hologram plate with the same coherent illumination and imaging at the same distance as the hologram was originally recorded. Therefore, the above formulation for recording is also valid for reconstruction. Since the hologram plate replaces the object plane, the transmittance function $1 - a(x,y)$ in the above formulas must be replaced by the amplitude transmittance of the hologram plate. Assuming that the recording medium has a linear characteristic, the amplitude transmittance of the hologram will be $e + bI_z(x,y)$, where e and b are constants. The constant b is negative for negative recording. Assuming a positive recording, the transmittance function can be rewritten as $d + I_z(x,y)$, with constants gathered in d. Therefore, the field at the imaging plane due to the illumination of the positive hologram is given by

$$\phi_z(x,y) = [d + I_z(x,y)] ** h_z(x,y) , \quad (12)$$

which is obtained by replacing $1 - a(x,y)$ of Eq. (5) by $d +$

$I_z(x,y)$. Equation (12) can be rewritten as

$$\phi_z(x,y) = d + I_z(x,y) ** h_z(x,y) \ . \tag{13}$$

Substituting Eq. (8) into this expression and expanding the components, we obtain

$$\phi_z(x,y) = d + 1 - a^*(x,y) ** h_z^*(x,y) ** h_z(x,y) - a(x,y) ** h_z(x,y) ** h_z(x,y) \ . \tag{14}$$

These components can be simplified using properties of $h_z(x,y)$ shown in the appendix:

$$h_{z_k}^*(x,y) ** h_{z_j}(x,y) = h_{z_j - z_k}(x,y) \ , \tag{15}$$

$$h_{z_k}(x,y) ** h_{z_j}(x,y) = h_{z_j + z_k}(x,y) \ , \tag{16}$$

$$h_0(x,y) = \delta(x,y) \ , \tag{17}$$

to yield

$$\phi_z(x,y) = d + 1 - a^*(x,y) ** \delta(x,y) - a(x,y) ** h_{2z}(x,y) = d - a^*(x,y) + [1 - a(x,y) ** h_{2z}(x,y)] \ . \tag{18}$$

Note that the second term is the desired reconstruction. The term in the brackets is exactly the field of a hologram of the object that would be present at a distance 2z, or twice the distance of the original recording. This term is the twin image. Thus, from Eqs. (5) and (18),

$$\phi_z(x,y) = d - a^*(x,y) + \psi_{2z}(x,y) \ . \tag{19}$$

It is impossible to observe or record the field in optical reconstructions. Only its intensity can be recorded. Therefore, the object reconstruction is taken to be proportional to the intensity of this field. This will yield additional undesired nonlinear components. In digital reconstruction, it is possible to compute and record the field directly. Note that the average level of the hologram $I(x,y)$ can be modified to improve the quality. For example, adding a large bias suppresses the nonlinear terms in the intensity of the reconstruction field $R_z(x,y)$, since

$$R_z(x,y) = \phi_z(x,y)\phi_z^*(x,y) = d^2 - 2\mathrm{Re}\{d a^*(x,y)\} - 2\mathrm{Re}\{d \psi_{2z}(x,y)\} + |a(x,y)|^2 + |\psi_{2z}(x,y)|^2 \ . \tag{20}$$

If d is large, then the last two terms are dominated.

The purpose of this paper is to present a new method for object reconstruction from in-line holograms that suppresses the twin image $\psi_{2z}(x,y)$. An algorithm is obtained by treating the reconstruction as an inverse problem. This algorithm is implemented digitally by computer. In this paper the basic structure of the algorithm, its digital implementation, and the results in particle field applications are presented.

3. THE RECONSTRUCTION ALGORITHM

We showed in the previous section that in-line hologram recording, as well as conventional reconstruction, can be modeled as a simple linear shift invariant 2-D system under the given assumptions (see Figs. 3 and 4). The system shown in Fig. 3 or in Fig. 4 can be converted to a discrete system and easily implemented digitally. In this case, if the input is a sampled object distribution $a(x,y)$, then the output will be the simulated sampled in-line hologram of that object. If the input is a digitized hologram, then the output will simulate the conventional reconstruction.

Taking as the goal the reconstruction of $a(x,y)$ from $I_z(x,y)$, the system model of Fig. 4 suggests the use of a system that inverts the forward transformation. Here we present a linear filter designed to decode the object $a(x,y)$ directly from its in-line hologram $I_z(x,y)$. The principal achievement of this approach is the suppression of the twin image. Furthermore, since the filtering operation is performed completely by digital means, the optical reconstruction step is eliminated.

Since the hologram $I_z(x,y)$ for real-valued $a(x,y)$ is given as the output of a linear system [see both Fig. 4 and Eq. (9)], a linear inverse filter is sought. The 2-D Fourier transform of the impulse response $g(x,y)$ (the frequency response) is given by

$$G(u,v) = \mathcal{F}\{2\mathrm{Re}\{h_z(x,y)\}\} = \mathcal{F}\left\{\frac{2}{\lambda z}\sin\frac{\pi}{\lambda z}(x^2+y^2)\right\} = 2\cos\frac{\lambda z}{4\pi}(u^2+v^2) \ , \tag{21}$$

where u and v are the transform domain variables. $G(u,v)$ has uncountably many zeros, so $1/G(u,v)$ does not exist. An inverse $\mathcal{G}(u,v)$ satisfying

$$1 - \mathcal{G}(u,v)G(u,v) = 0 \quad \forall (u,v) \in \mathbf{R}^2 \tag{22}$$

cannot be found. However, we can find an $\mathbf{L}_2$ inverse $\mathcal{G}(u,v)$ satisfying

$$\int_{-\infty}^{\infty}\int_{-\infty}^{\infty} |1 - \mathcal{G}(u,v)G(u,v)|^2 du dv = 0 \ . \tag{23}$$

It is proved in Ref. 16 that the filter given by

$$\mathcal{G}_M(u,v) = \cos\frac{\lambda z}{4\pi}(u^2+v^2) + \sum_{k=1}^{2^{M-1}-1} \frac{M - 1 - [\![\log_2 k]\!]}{M} S_k(u,v) \ , \tag{24}$$

$$S_k(u,v) = (-1)^k \cos\frac{\lambda z}{4\pi}(2k+1)(u^2+v^2) \ ,$$

is a series approximation to the desired inverse and converges to it in the energy or $\mathbf{L}_2$ metric (23) as $M \to \infty$. Application of this linear filter with any finite M to the hologram yields a constant term and a residual error term in addition to the desired reconstructed object. It is not desirable to approximate the exact inverse too closely, since for large M such a function inherits the same undesirable properties as the true inverse, most notably high gain near the zeros of $G(u,v)$. In our experience M selected in the range 3 to 5 works satisfactorily for particle field holograms. For $M = 1$ (first-order

approximation) the approximate inverse filter, Eq. (24), is equivalent to the conventional reconstruction since

$$2\mathcal{G}_1(u,v) = G(u,v) \ . \tag{25}$$

Additional terms tend to enhance suppression of the twin image and thus improve the quality of the reconstruction. As more terms are added, however, the residual twin image rapidly declines in rms value, and further improvement must be traded off against small but inevitable degradations due to finite word length and modeling errors.

4. PHYSICAL INTERPRETATION OF THE TRUNCATED INVERSE FILTER

The truncated inverse filter as defined by Eq. (24) may be given a physical interpretation. In fact, the main result summarized in Eq. (24) was discovered as a consequence of formalizing the arguments presented in this section.

For real-valued $a(x,y)$, the real and imaginary parts of the field given by Eq. (18) are

$$\begin{aligned} \mathrm{Re}\{\phi_z(x,y)\} &= d + 1 - a(x,y) - a(x,y) ** \mathrm{Re}\{h_{2z}(x,y)\} \\ &\triangleq d + 1 + b_z(x,y) \ , \end{aligned} \tag{26}$$

$$\begin{aligned} \mathrm{Im}\{\phi_z(x,y)\} &= -a(x,y) ** \mathrm{Im}\{h_{2z}(x,y)\} \\ &\triangleq q_z(x,y) \ . \end{aligned} \tag{27}$$

The desired component $a(x,y)$ is present in the real part $b_z(x,y)$. In addition, $b_z(x,y)$ has the real part of the twin image superposed to $a(x,y)$. On the other hand, $q_z(x,y)$ consists of only the imaginary part of the twin image. A useful observation is that $q_z(x,y)$ is itself very similar to a hologram, with the distance parameter $2z$; $\mathrm{Im}\{h_{2z}(x,y)\}$ is the convolution kernel, instead of $\mathrm{Re}\{h_z(x,y)\}$ [see Eq. (9)]. So we can use $q_z(x,y)$ as if it were a new hologram containing added (quadrature) information to be reconstructed. In fact, using the properties cited in the appendix,

$$\mathrm{Im}\{h_{kz}(x,y)\} ** \mathrm{Im}\{h_{kz}(x,y)\} = \frac{1}{2}\delta(x,y) - \frac{1}{2}\mathrm{Re}\{h_{2kz}(x,y)\} \ , \tag{28}$$

$$\mathrm{Im}\{h_{kz}(x,y)\} ** \mathrm{Re}\{h_{kz}(x,y)\} = \frac{1}{2}\mathrm{Im}\{h_{2kz}(x,y)\} \ , \tag{29}$$

the propagating components of this "quadrature hologram" can be computed at $2z$ as

$$\begin{aligned} & q_z(x,y) ** 2\mathrm{Im}\{h_{2z}(x,y)\} \\ &= -2a(x,y) ** \mathrm{Im}\{h_{2z}(x,y)\} ** \mathrm{Im}\{h_{2z}(x,y)\} \\ &= -a(x,y) ** \delta(x,y) + a(x,y) ** \mathrm{Re}\{h_{4z}(x,y)\} \\ &= -a(x,y) + a(x,y) ** \mathrm{Re}\{h_{4z}(x,y)\} \\ &\triangleq p_{2z}(x,y) \ , \end{aligned} \tag{30}$$

$$\begin{aligned} & q_z(x,y) ** 2\mathrm{Re}\{h_{2z}(x,y)\} \\ &= -2a(x,y) ** \mathrm{Im}\{h_{2z}(x,y)\} ** \mathrm{Re}\{h_{2z}(x,y)\} \\ &= -a(x,y) ** \mathrm{Im}\{h_{4z}(x,y)\} \\ &= q_{2z}(x,y) \ . \end{aligned} \tag{31}$$

In fact, p and q of doubled order may be computed recursively together:

$$p_{2^n z}(x,y) = q_{2^{n-1}z}(x,y) ** 2\mathrm{Im}\{h_{2^n z}(x,y)\} \ , \tag{32}$$

$$q_{2^n z}(x,y) = q_{2^{n-1}z}(x,y) ** 2\mathrm{Re}\{h_{2^n z}(x,y)\} \ , \tag{33}$$

At each recursion of Eqs. (32) and (33), a new reconstruction $p_{2^n z}(x,y)$ that contains the desired component $-a(x,y)$ is made. All of these reconstructions have a twin image contaminating the desired image component. But the twin images at every stage n are different from each other. They are the holograms (real parts) that would be observed at different distances $2^{n+1}z$. Suppose that the average of all reconstructions, that is, all $p_{2^n z}(x,y)$'s and $b_z(x,y)$, is taken. Since all of these terms have the desired component in them, the average will contain this component. However, since the twin-image terms are different in scale, they do not add constructively; in fact, they tend to exactly cancel each other everywhere. Thus, taking the average, we have

$$\begin{aligned} d_M(x,y) &= \frac{1}{M}\left[b_z(x,y) + \sum_{n=1}^{M-1} p_{2^n z}(x,y)\right] \\ &= -a(x,y) + a(x,y) ** \frac{1}{M}\left[-\mathrm{Re}\{h_{2z}(x,y)\} + \sum_{n=1}^{M-1} \mathrm{Re}\{h_{2^{n+1}z}(x,y)\}\right] . \end{aligned} \tag{34}$$

It can be shown that the convolution kernel of Eq. (34) converges uniformly to zero as $M \to \infty$.[16] If $a(x,y)$ has finite energy, then

$$\lim_{M \to \infty} d_M(x,y) = -a(x,y) \ , \tag{35}$$

which is the desired decoding with no residual twin-image term.

This algorithm is analogous to having recorded thin planar holograms from a volume hologram at distances $2^k z$, for $k = 0, 1, 2, \ldots$. As the number of planes increases, the net effect is twin-image suppression, as is expected for volume hologram reconstruction. In the present case, only one thin planar hologram is recorded, but the equivalent of the series of double distance holograms is obtained from the single recorded hologram by digital computation.

It can be shown that the truncated inverse filter described in Sec. 3 [Eq. (24)] is exactly equivalent to the iterative doubling procedure of this section. The algorithm is summarized in Fig. 5.

5. DIGITAL IMPLEMENTATION OF THE TRUNCATED INVERSE FILTER

The truncated inverse filter can be efficiently implemented in the Fourier transform domain. The Fourier transforms of the functions given in Fig. 5 are

$$\mathcal{F}\{\mathrm{Re}\{h_{kz}(x,y)\}\} = \cos\frac{\lambda k z}{4\pi}(u^2 + v^2) \ , \tag{36}$$

$$\mathcal{F}\{\mathrm{Im}\{h_{kz}(x,y)\}\} = -\sin\frac{\lambda k z}{4\pi}(u^2 + v^2) \ . \tag{37}$$

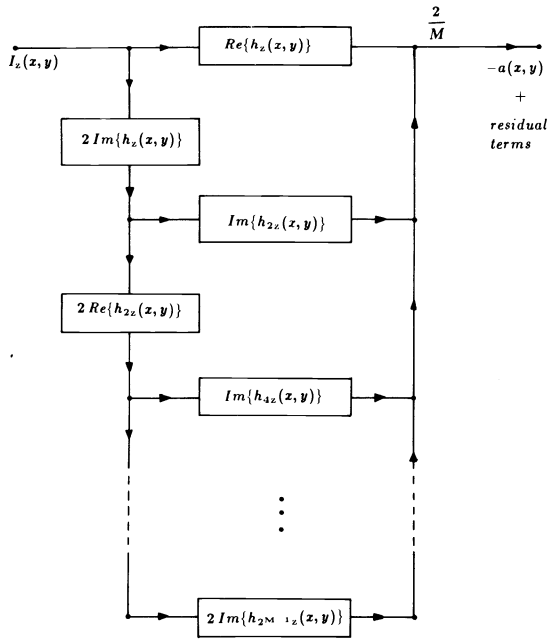

Fig. 5. The truncated inverse filter for decoding in-line holograms.

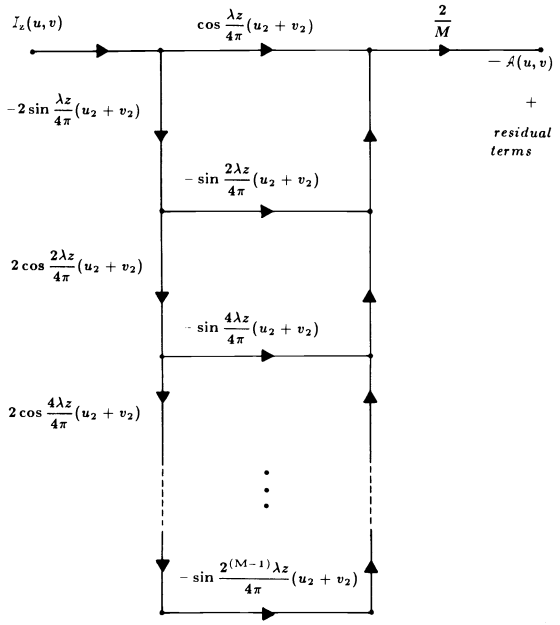

Fig. 6. The truncated inverse filter in the Fourier transform domain.

The filter shown in Fig. 5 can be represented in the Fourier domain as shown in Fig. 6. The structure given in Fig. 6 for the computation of the filter is more efficient than the direct implementation of Eq. (24). Digital decoding of in-line holograms, which suppresses the twin image, is achieved by the digital implementation of the filter shown in Fig. 6. Note that the truncated inverse filter as shown in Figs. 5 and 6 is neither band limited nor space limited. However, because of the linearity of the system, the filter needs to be considered only over the passband of the input. The input can be assumed to be a low-pass function with cutoff frequency determined by the experimental parameters or by the desired resolution. Therefore, the filter of Fig. 5 can be band limited without

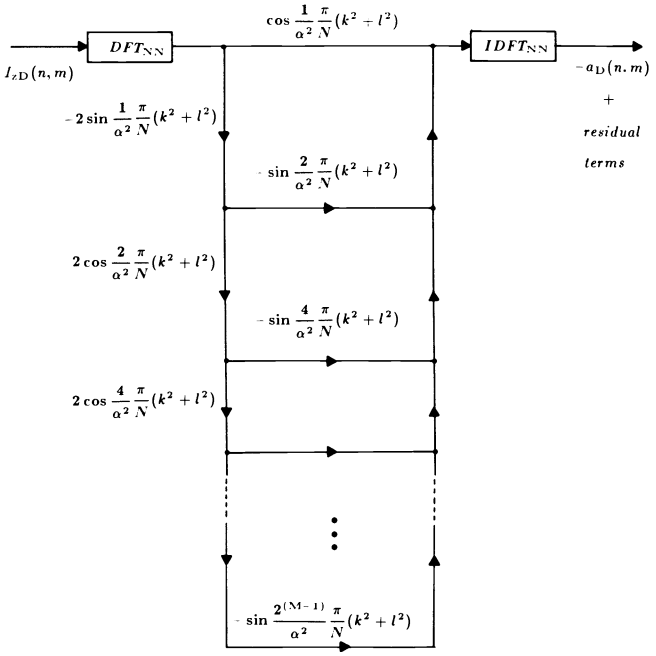

Fig. 7. Digital implementation of the truncated inverse filter.

degrading the resolution, if its passband is limited to the passband of the object function. Because of the specific form of the kernel, its band-limited version is also *almost* space limited. Thus, once the resolution limit of the object distribution is set, both the sampling rate and the spatial extent of the filter are known. This information is enough to convert the continuous system given in Figs. 5 and 6 to a discrete system. For computational efficiency, circular convolutions are used instead of linear convolutions.

The discrete version of the convolution kernel $h_z(x,y)$ is given as

$$h_z(n,m) = K\exp\left[j\frac{\pi}{\lambda z}X^2(n^2+m^2)\right]$$

$$= K\exp\left[j\alpha^2\frac{\pi}{N}(n^2+m^2)\right], \tag{38}$$

where X is the spatial sampling period. The parameter α is introduced for normalization and is defined as

$$\alpha^2\frac{\pi}{N} = \frac{\pi}{\lambda z}X^2 . \tag{39}$$

Full discussion of issues related to sampling and discretization of holograms may be found in Refs. 16 and 17. The discrete implementation of the truncated inverse filter is shown in Fig. 7.

6. RESULTS

The algorithm shown in Fig. 7 has been implemented in the image processing laboratory of the Laboratory for Power and Environmental Studies of the State University of New York at Buffalo. The laboratory is equipped with a Comtal Vision One/20 image processor interfaced with a bank of VAX 11 minicomputers. A TV camera, magnifying lenses, and a light table are used to input optical holograms. For the following figures, the initial hologram sizes are 256×256 pixels, with

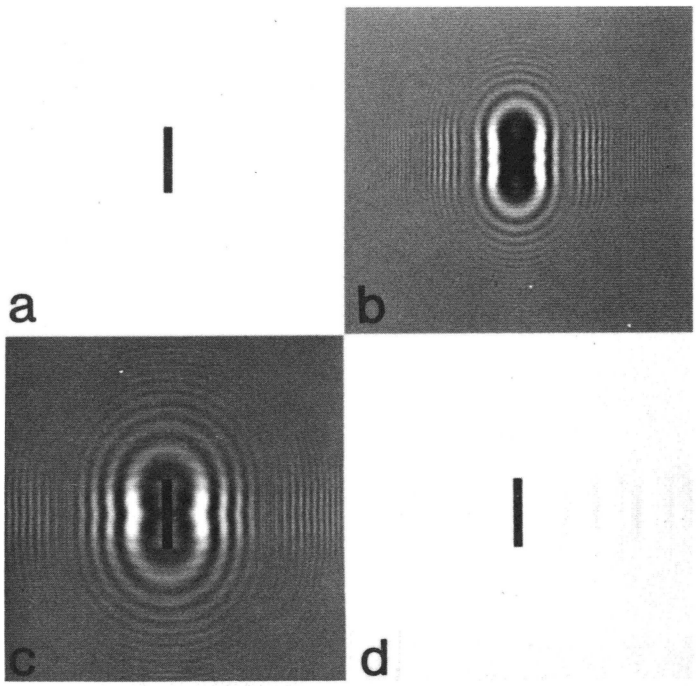

Fig. 8. (a) A computer-synthesized object. (b) Simulated in-line hologram of the object of (a); $\alpha = 1$. (c) Conventional reconstruction by computation from the hologram of (b). (d) Reconstruction from the hologram of (b) using the truncated inverse filter; M = 5.

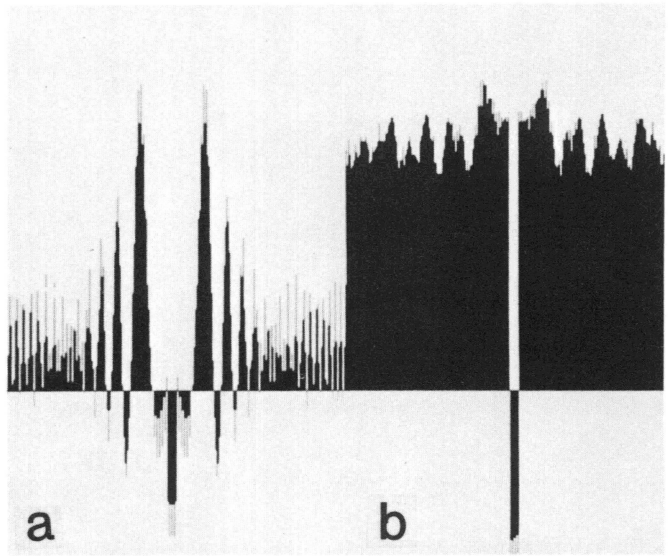

Fig. 9. (a) Intensity profile of Fig. 8(c) and (b) intensity profile of Fig. 8(d) along horizontal lines passing through their centers. The ordinate is scaled linearly in the gray-level range of the corresponding image, with level 255 (brightest white) at top and level 0 (black) at bottom. Fill gray-level reverses at level 127. Note the reduced variation surrounding the reconstructed object in (b).

256 gray levels per pixel. The size of the discrete Fourier transform pair used for the circular convolutions is 512×512.

Figure 8 shows a computer-simulated in-line hologram of a rectangular object, together with its conventional reconstruction and a reconstruction employing the procedure described in this paper. The reconstruction obtained in Fig. 8(d) is obtained directly from the hologram of Fig. 8(b) by a truncated inverse filter with $M = 5$. Profiles of the reconstructions of Figs. 8(c) and 8(d) are shown in Figs. 9(a) and 9(b), respectively. The peak-to-peak level of the background artifact is reduced by a factor of 8.0 in Fig. 8(d) compared to Fig. 8(c). The reduction is 5 times in the rms sense.

Figure 10(a) shows an optical hologram of deposited particles. The particle size range is 10 to 30 μm, and the recording distance is 1.3 cm. Figure 10(b) is the computer simulation of the conventional reconstruction from this hologram. The same hologram can be reconstructed with approximate inverse filtering to suppress the twin image. The result for $M = 3$ is shown in Fig. 10(c).

The importance of the reduction of the background artifact by suppressing the twin image is demonstrated by Fig. 11. Most workers agree that fully automated analysis of in-line holograms would be desirable. Such automation would require several processing levels. In the image processing phase, the hologram is enhanced and decoded in preparation for higher level pattern recognition and analysis. Simple nonlinear operations may be used as postprocessors, operating on the results of truncated inverse filtering to complete the image processing phase. Such nonlinear operations cannot perform well if they are used on images produced by conventional optical reconstruction. Figure 11 shows the results of simple thresholding to binarize the output images. Figure 11(a) corresponds to Fig. 10(c), and Fig. 11(b) corresponds to Fig. 10(b). Another simple nonlinear postprocessor is the covariance filter for edge detection.[16] The result of a cascaded processing of the hologram of Fig. 12(a) by approximate inverse filtering and subsequent edge detection by a covariance filter is shown in Fig. 12(b). This figure summarizes the work reported in this study. The decoded figure [12(b)] is obtained from its in-line hologram [12(a)] completely by digital means.

7. CONCLUSIONS

Digital and optical data processing techniques have characteristics that are often complementary to each other, stimulating interest in the development of systems combining both digital and optical subsystems. While optical processing offers fast, massively parallel data acquisition and transformation, the flexibility of digital computation can often be exploited to produce transformations that are nonphysical or at best very difficult to produce in the analog world. Here, such a hybrid system is employed for optical encoding and digital decoding of Fresnel or far-field in-line holograms. The intrinsic high resolution in space and time, depth of field, and robustness of in-line holography remains available, without the usual limitations associated with optical reconstruction. The advantages of digital decoding (twin-image suppression, automated data reduction, no far-field requirement) must of course be weighed against the added costs of digital processing. In our experience, these added costs are frequently well compensated for by bypassing the tedious and subjective process of conventional optical reconstructions in many particle and aerosol applications.

8. APPENDIX: SOME RELATED FORMULAS

In the formulas below, $\mathcal{F}$ and $\mathcal{F}^{-1}$ denote the 2-D Fourier and inverse Fourier transforms, respectively.

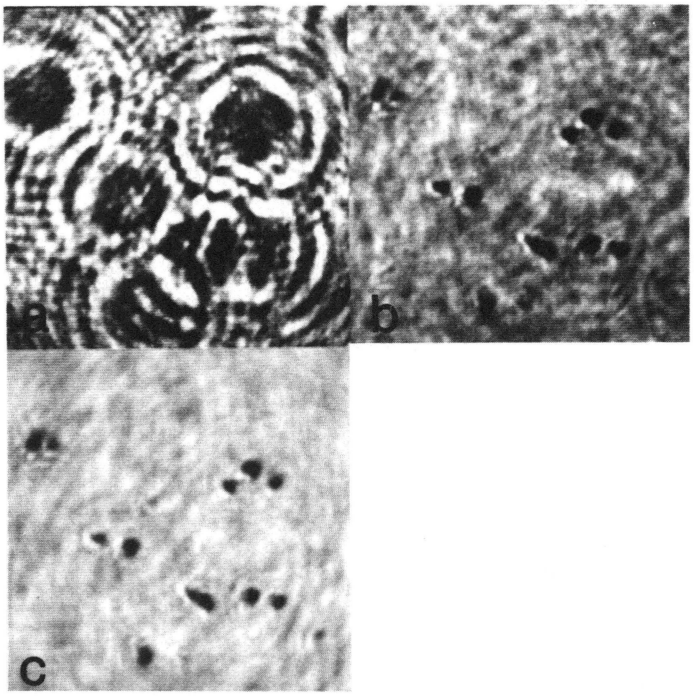

Fig. 10. (a) A portion of an optical in-line hologram. (b) Conventional reconstruction from the hologram of (a); $\alpha = 0.541$. (c) Reconstruction from the hologram of (a) using the truncated inverse filter; M = 3.

Fig. 11. Thresholding applied to (a) the reconstruction of Fig. 10(c) and (b) the reconstruction of Fig. 10(b).

(1)

$$\mathcal{F}\{\exp[ja(x^2+y^2)]\} = j\frac{\pi}{a}\exp\left(-j\frac{u^2+v^2}{4a}\right), \tag{A1}$$

$$\mathcal{F}\{\cos a(x^2+y^2)\} = \frac{\pi}{a}\sin\frac{u^2+v^2}{4a}, \tag{A2}$$

$$\mathcal{F}\{\sin a(x^2+y^2)\} = \frac{\pi}{a}\cos\frac{u^2+v^2}{4a}. \tag{A3}$$

(2)

$$h_z(x,y) = \frac{1}{j\lambda z}\exp\left[j\frac{\pi}{\lambda z}(x^2+y^2)\right], \tag{A4}$$

$$\mathcal{F}\{h_z(x,y)\} = \exp\left[-j\frac{\lambda z}{4\pi}(u^2+v^2)\right] = H_z(u,v), \tag{A5}$$

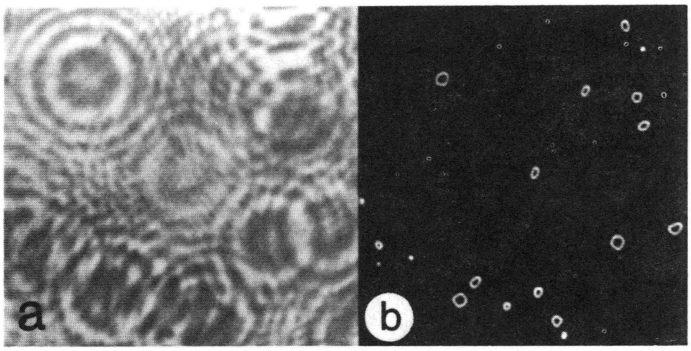

Fig. 12. Digital decoding of an optical in-line hologram: (a) optical hologram and (b) result of edge detection (output of the covariance filter) applied to the reconstruction using the truncated inverse filter.

$$\mathcal{F}\{\mathrm{Re}\{h_z(x,y)\}\} = \cos\frac{\lambda z}{4\pi}(u^2+v^2), \tag{A6}$$

$$\mathcal{F}\{\mathrm{Im}\{h_z(x,y)\}\} = -\sin\frac{\lambda z}{4\pi}(u^2+v^2). \tag{A7}$$

(3)

$$1 ** h_z(x,y) = H_z(0,0)\cdot 1 = 1, \tag{A8}$$

$$\begin{aligned} h^*_{z_k}(x,y) ** h_{z_j}(x,y) &= \mathcal{F}^{-1}\left\{\exp\left[j\frac{\lambda}{4\pi}z_k(u^2+v^2)\right]\right. \\ &\quad \left.\times\exp\left[-j\frac{\lambda}{4\pi}z_j(u^2+v^2)\right]\right\} \\ &= \mathcal{F}^{-1}\left\{\exp\left[-j\frac{\lambda(z_j-z_k)}{4\pi}(u^2+v^2)\right]\right\} \\ &= h_{z_j-z_k}(x,y), \end{aligned} \tag{A9}$$

$$\begin{aligned} h_{z_k}(x,y) ** h_{z_j}(x,y) &= \mathcal{F}^{-1}\left\{\exp\left[-j\frac{\lambda}{4\pi}z_k(u^2+v^2)\right]\right. \\ &\quad \left.\times\exp\left[-j\frac{\lambda}{4\pi}z_j(u^2+v^2)\right]\right\} \\ &= \mathcal{F}^{-1}\left\{\exp\left[-j\frac{\lambda(z_j+z_k)}{4\pi}(u^2+v^2)\right]\right\} \\ &= h_{z_j+z_k}(x,y), \end{aligned} \tag{A10}$$

$$\begin{aligned} h^*_z(x,y) ** h_z(x,y) &= \mathcal{F}^{-1}\left\{\exp\left[j\frac{\lambda}{4\pi}z(u^2+v^2)\right]\right. \\ &\quad \left.\times\exp\left\{-j\frac{\lambda}{4\pi}z(u^2+v^2)\right]\right\} \\ &= \mathcal{F}^{-1}\{1\} \\ &= \delta(x,y). \end{aligned} \tag{A11}$$

(4)

$$\mathrm{Im}\{h_{kz}(x,y)\} ** \mathrm{Im}\{h_{kz}(x,y)\} = \mathcal{F}^{-1}\left\{\left[-\sin\frac{\lambda kz}{4\pi}(u^2+v^2)\right] \times\left[-\sin\frac{\lambda kz}{4\pi}(u^2+v^2)\right]\right\}$$

$$= \mathcal{F}^{-1}\left\{\frac{1}{2}-\frac{1}{2}\cos\frac{\lambda 2kz}{4\pi}(u^2+v^2)\right\}$$

$$= \frac{1}{2}\delta(x,y)-\frac{1}{2}\,\mathrm{Re}\{h_{2kz}(x,y)\} \quad \text{(A12)}$$

$$\mathrm{Im}\{h_{kz}(x,y)\} ** \mathrm{Re}\{h_{kz}(x,y)\} = \mathcal{F}^{-1}\left\{\left[-\sin\frac{\lambda kz}{4\pi}(u^2+v^2)\right] \times\left[\cos\frac{\lambda kz}{4\pi}(u^2+v^2)\right]\right\}$$

$$= \mathcal{F}^{-1}\left\{-\frac{1}{2}\sin\frac{\lambda 2kz}{4\pi}(u^2+v^2)\right\}$$

$$= \frac{1}{2}\,\mathrm{Im}\{h_{2kz}(x,y)\}\ . \quad \text{(A13)}$$

9. REFERENCES

1. J. D. Trolinger, "Particle and flow field holography: a critical survey," in *Holography*, L. Huff, ed., Proc. SPIE 532, 40–62 (1985).
2. B. J. Thompson, "Diffraction by opaque and transparent particles," J. Soc. Photo-Optical Instrumentation Engineers 2(2), 43–46 (1963).
3. G. B. Parrent and B. J. Thompson, "On the Fraunhofer (far-field) diffraction patterns of opaque and transparent objects with coherent background," Opt. Acta 11, 183–192 (1964).
4. B. J. Thompson, "A new method of measuring particle size by diffraction techniques," Jpn. J. Appl. Phys. 4, Suppl. 1, 302–307 (1965).
5. B. J. Thompson, "Holographic particle sizing techniques," J. Phys. E 7, 781–788 (1974).
6. B. J. Thompson and P. Dunn, "Advances in far-field holography—theory and applications," in *Recent Advances in Holography*, T.-C. Lee and P. N. Tamura, eds., Proc. SPIE 215, 102–111 (1980).
7. R. J. Collier, C. B. Burckhardt, and L. H. Lin, *Optical Holography*, Academic Press, New York (1971).
8. H. J. Caulfield, "Automated analysis of particle holograms," Opt. Eng. 24(3), 462–463 (1985).
9. R. Bexon, J. Gibbs, and G. D. Bishop, "Automatic assessment of aersol holograms," J. Aerosol Sci. 7, 397–407 (1976).
10. K. H. S. Marie, J. C. Bennet, and A. P. Anderson, "Digital processing technique for suppressing the interfering outputs in the image from an in-line hologram," Electron. Lett. 15, 241–243 (1979).
11. G. Liu and P. D. Scott, "Phase retrieval and twin-image elimination for in-line Fresnel holograms," J. Opt. Soc. Am. A 4, 159–165 (1987).
12. J. W. Goodman, *Introduction to Fourier Optics*, McGraw-Hill, New York (1968).
13. L. M. Soroko, *Holography and Coherent Optics*, Plenum Press, New York (1968).
14. A. Papoulis, *Systems and Transformations with Applications in Optics*, McGraw-Hill, New York (1968).
15. G. A. Tyler and B. J. Thompson, "Fraunhofer holography applied to particle size analysis: a reassessment," Opt. Acta 23, 685–700 (1976).
16. L. Onural, "Digital decoding of in-line holograms," Ph.D. dissertation, State Univ. of New York at Buffalo (1985).
17. L. P. Yaroslavskii and N. S. Merzlyakov, *Methods of Digital Holography* (translated from the Russian by D. Parsons), Consultants Bureau, New York (1980).

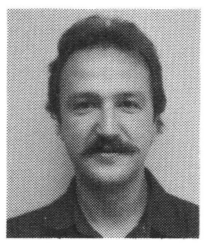

Levent Onural was born in Izmir, Turkey, in 1957. He received the BS (high honors) and MS degrees in electrical engineering from the Middle East Technical University, Ankara, Turkey, in 1979 and 1981, respectively, and the Ph.D. degree in electrical and computer engineering from the State University of New York at Buffalo in 1985. He has been a Fullbright Scholar since 1981. In 1985 he was appointed research assistant professor at the State University of New York at Buffalo, and in 1986 joined the Electrical and Electronics Engineering Department of Bilkent University, Ankara, Turkey, as an assistant professor. His research interests include signal processing, image processing, holography, and fractal models. Dr. Onural is a member of IEEE.

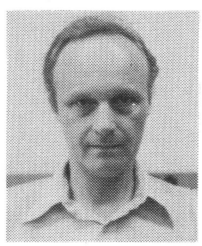

Peter D. Scott received the BS, MS, and Ph.D. degrees from the Phillips School of Electrical Engineering, Cornell University, in 1966, 1968, and 1970, respectively. He has served as an assistant professor and an associate professor in the Department of Electrical and Computer Engineering, State University of New York at Buffalo, since 1970 and since 1976 has held a joint appointment with the School of Biophysical Sciences at SUNY at Buffalo. Dr. Scott's current research interests include digital image processing, biomedical signal analysis, and digital holography.